HHS Public Access

Author manuscript

Nano Res. Author manuscript; available in PMC 2019 October 25.

Published in final edited form as:

Nano Res. 2018 ; 11(10): 5573–5583. doi:10.1007/s12274-018-2084-y.

Cell membrane coating for reducing nanoparticle-induced inflammatory responses to scaffold constructs

Zhiyuan Fan[#1], **Peter Y. Li**[#1], **Junjie Deng**[1,2], **Stephen C. Bady**[1], **Hao Cheng**[1]

[1]Department of Materials Science and Engineering, Drexel University, Philadelphia, Pennsylvania 19104, USA

[2]Engineering Research Center of Clinical Functional Materials and Diagnosis & Treatment Devices of Zhejiang Province, Wenzhou Institute of Biomaterials and Engineering, CAS, Wenzhou 325011, China

[#] These authors contributed equally to this work.

Abstract

The controlled release of therapeutics from micro or nanoparticles has been well-studied. Incorporation of these particles inside biomaterial scaffolds is promising for tissue regeneration and immune modulation. However, these particles may induce inflammatory and foreign body responses to scaffold constructs, limiting their applications. Here we show that widely used poly(lactic-co-glycolic acid) nanoparticles (PLGA NPs) formed by double emulsion dramatically increased neutrophil infiltration and pro-inflammatory cytokines in alginate scaffolds 1 day after the subcutaneous injection of the scaffolds into mice. The coating of red blood cell (RBC) membranes on PLGA NPs completely eliminated these short-term inflammatory responses. For a longer term of 10 days, neither PLGA NPs nor RBC membrane-coated nanoparticles exerted a significant effect on the infiltration of neutrophils or macrophages in alginate scaffolds possibly due to the degradation and/or clearance of nanoparticles by infiltrating cells by that time. Despite the extensive exploration of cell membrane-coated nanoparticles, our study is the first to investigate the effects of cell membrane coating on foreign body reaction to nanoparticles. Harnessing the natural biocompatibility of cell membranes, our strategy of anti-inflammatory protection for scaffolds may be pivotal for many applications, such as those relying on the recruitment of stem cells and/or progenitor cells to scaffolds.

Graphical Abstract

Incorporation of therapeutic-releasing nanoparticles into biomaterial scaffolds has broad applications in tissue regeneration and immune modulation, but may induce excessive inflammatory and foreign body responses to scaffold constructs, limiting their applications. We report a new strategy to harness the natural biocompatibility of cell membranes to eliminate the acute inflammatory responses by coating nanoparticle surfaces with red blood cell membranes.

Address correspondence to hcheng@drexel.edu.

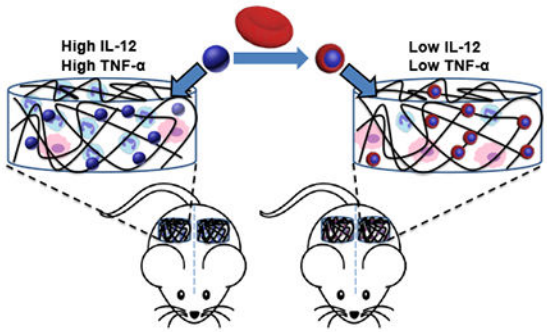

Keywords

Regenerative medicine; wound healing; drug delivery; endothelial cells; immune tolerance

1 Introduction

Stem cells and biomaterial scaffolds are two cornerstones of regenerative medicine [1, 2]. Scaffolds that release cytokines, growth factors, and other therapeutics to recruit and modulate cells or control cell microenvironments *in situ* have attracted increasing attention and are a promising modality for tissue regeneration and immune modulation [3–13]. One popular strategy for controlled release of therapeutics from scaffolds is the incorporation of therapeutic-encapsulated microparticles or nanoparticles into scaffolds [14–17]. This approach is particularly important when the therapeutics are peptides or small molecules, and scaffold polymers are hydrophilic. Unlike proteins, controlled release of relatively small molecules cannot be achieved by entrapping them inside crosslinked hydrophilic polymers. Although it has not been extensively studied, it is known that nanoparticles inside highly biocompatible scaffolds can cause excessive inflammatory responses to scaffold constructs, for example increased neutrophil infiltration [18]. Despite the fact that an appropriate inflammatory response is necessary for wound healing and may be helpful for stimulating immune responses of scaffold-based vaccines [3, 19], uncontrolled inflammatory responses should be minimized for general tissue regeneration [20].

Acute inflammation is the first stage of the foreign body reaction to implanted/injected scaffolds that are recognized as “foreign” by the host immune system. As soon as scaffolds are placed inside animals or humans, proteins start to adsorb onto scaffold materials. Protein adsorption can activate coagulation and complement cascades that further stimulate immune cells [20–23]. Highly biocompatible materials such as zwitterionic polymers, alginate, and its derivatives are mostly superhydrophilic with ultralow protein adsorption [24, 25]. In addition to minimizing protein adsorption, scaffolds may be camouflaged to attenuate inflammatory and foreign body responses. Biomaterials cloaked with “self” proteins such as CD200 have shown reduced foreign body reaction [26], while the modification of materials with peptides binding to Factor H, a soluble complement inhibitory protein, effectively diminished materials-induced complement activation [27].

Recently, cell membrane-coated nanoparticles have emerged as a new class of nanomaterials [28–37]. Cell membrane coating enables the camouflage of nanoparticles for evading immune clearance and the utilization of natural membrane bound receptors for active targeting or other applications. Red blood cell (RBC) membranes are rich in “self” protein CD47, which downregulates macrophage phagocytosis via binding to signal regulatory protein alpha on the cells [38]. Cell membrane coating can also lessen complement activation by nanoparticles [29]. We thus hypothesized that an RBC membrane cloak around nanoparticles would attenuate nanoparticle-induced inflammatory responses to scaffold constructs. Here, we report the incorporation of double-emulsion poly(lactic-co-glycolic acid) nanoparticles (PLGA NPs), which are widely used for encapsulating cytokines, growth factors, peptides, and hydrophobic drugs, into a macroporous alginate scaffold. PLGA NPs dramatically increased the infiltrated neutrophils and inflammatory cytokines inside scaffolds *in vivo* (Fig. 1). This early stage inflammatory response was eliminated after coating PLGA NPs with RBC membranes. Recent studies on cell membrane- coated nanoparticles mostly have focused on targeted delivery, whereas our study is the first to explore the application of cell membrane coating in reducing inflammatory and foreign body responses to nanoparticles.

2 Experimental

2.1 Synthesis of methacrylate-alginate (MA-alginate)

To synthesize MA-alginate, ultra-pure alginate (0.15 g, PRONOVA SLM100) was dissolved in 15 mL DI water in a round flask under stirring. After the alginate was fully dissolved, the flask was put in an ice-water bath. Methacrylic anhydride (11.73 g) was added dropwise into the flask, and the solution was stirred vigorously to make the solution homogeneous. Sodium hydroxide water solution (7.5 M, Fisher Scientific) was used to adjust the pH value to 8 as monitored by pH papers. After 24 h, the solution was added dropwise to ethanol (Decon, 200 proof) to precipitate the MA-alginate. MA-alginate was collected by centrifugation and washed three times with ethanol. The pellet was dried under vacuum overnight to remove ethanol. Afterwards, it was redissolved in DI water and dialyzed using Snake Skin Dialysis Tubing (Thermo Scientific, 10K MWCO) against water for 2 days. The solution was then lyophilized to obtain MA-alginate. The polymer was dissolved in deuterium oxide and characterized by ^{1}H NMR spectrum on 500MHz Varian. ^{1}H NMR (δ, D_2O): 6.12 and 5.80 (2H, CH_2=CCH$_3$), 1.92 (3H, CH$_2$=CCH_3), 3.45-4.40 (5H, in the repeating unit of alginate). The degree of substitution (DS) of MA-alginate was assessed by ^{1}H NMR analysis according to Eq 1, where $I_{1.92}$ is the integral of proton resonance signal at δ = 1.92 ppm, $I_{3.45\text{-}4.40}$ is the integral of proton resonance signals at δ=3.45-4.40 ppm.

$$\mathrm{DS} = \left(5 \times I_{1.92}\right) / \left(3 \times I_{3.45-4.40}\right) \times 100\,\% \quad (1)$$

2.2 Fabrication of PLGA NPs using a double emulsion method

PLGA NPs were prepared following a previously reported double emulsion method [29]. In brief, carboxyl-terminated PLGA (50:50) with inherent viscosity of 0.66 dL/g (Durect Co. Birmingham Division, USA) was dissolved in dichloromethane at 10 mg/mL. Then, 50 μL of Tris-HCl buffer (0.5 M, pH 8.0) was added dropwise to 1 mL PLGA solution in a clean glass vial. The solution was sonicated by a probe sonicator (Fisher Sonic Dismembrator) (30% amplitude, 1 min, pulse: 2 s on and 1 s off) on ice. After sonication, 5 mL of Tris-HCl buffer (0.01 M, pH 8.0) was added to the emulsified solution, and the solution was sonicated again under the aforementioned condition. Afterwards, the solution was transferred to a glass vial with 10 mL of Tris-HCl buffer (0.01 M, pH 8.0), and the solution was stirred overnight to remove the organic solvent. PLGA NPs were collected by centrifugation at 15,000 × g for 15 min at 4 °C and washed once in DI H_2O. The collected PLGA NPs were resuspended in DI H_2O for future steps. In order to quantify the particle loss during the washing steps, 1,1'-dioctadecyl-3,3,3',3'-tetramethyl-indodicarbocyanine, 4-chlorobenzenesulfonate salt (DiD) (Life Technologies) was used to label PLGA NPs. To fabricate DiD-labeled PLGA NPs, DiD was added to the PLGA dichloromethane solution at 0.05 wt% prior to emulsion. Fluorescence intensity at 650 nm with an excitation at 620 nm was used to quantify nanoparticles.

2.3 Preparation of RBC membrane-coated PLGA NPs

A sub-mandibular blood collection method was used to collect blood from C57BL/6J mice (Jackson Laboratory). All animal procedures were conducted according to the protocols approved by the Drexel University Institutional Animal Care and Use Committee in compliance with NIH guidelines. The blood was spun down at 300 × g for 5 min, and then the plasma and buffy coat were carefully removed. After washing RBCs three times with PBS to remove free proteins, EDTA water solution (0.2 nM) was used to rupture RBC membranes and the solution was adjusted back to 1 × PBS using 10 × PBS (Lonza). The solution was centrifuged at 18,000 × g for 6 min to spin down the membranes, and the supernatant was removed. This process was repeated until the membrane pellet became a transparent white color. In order to obtain membrane vesicles, membranes in water were sonicated with a probe sonicator at 20% power output for 1 s. One mg of PLGA NPs were mixed with RBC membrane vesicles from 100 μL of blood. This mixture was kept at 4 °C overnight to produce RBC membrane-coated PLGA NPs (RBCM-PLGA NPs). RBCM-PLGA NPs were collected by centrifugation at 15,000 × g for 15 min at 4 °C. The supernatant with excess RBC membranes was removed, and the pellet was resuspended in DI H_2O at a concentration of 50 mg/ml for next steps.

2.4 Preparation of MA-alginate scaffolds

Macroporous MA-alginate scaffolds were prepared via a cryogelation method, in which MA-alginate was chemically crosslinked at −20 °C [39]. MA-alginate was dissolved in DI water to make a 1% wt solution. For 50 μl of MA-alginate solution, 0.32 μL of tetramethylethylenediamine (TEMED, Fisher Scientific) was added and mixed well with the solution. Then 1.25 μL of 10% ammonium persulfate (APS, Fisher Scientific) water solution was added. After mixing, the solution was transferred to a 1 mL syringe (BD, USA) and

immediately placed in a −20 °C freezer for at least 12 h to form a disc-shaped scaffold. Afterwards, the scaffold was thawed and removed from the syringe, washed in 5 mL DI water for 1 h to remove the APS and TEMED used for crosslinking. The scaffold was then lyophilized. In order to load nanoparticles, each scaffold was rehydrated with either 40 μL PLGA NP solution (50 mg/mL in H_2O) or RBCM-PLGA NP solution (50 mg/mL in H_2O) for 30 min. The scaffolds were then lyophilized again and stored for further studies.

2.5 Characterization of nanoparticles and scaffolds

The size and surface potential of PLGA NPs and RBCM-PLGA NPs in H_2O were tested using a Zetasizer Nano ZS (Malvern Instruments, UK). The morphology of particles was imaged using transmission electron microscope (TEM). Samples were prepared as following: plasma was used to clean a carbon film-coated copper grid, and 10 μL of nanoparticle solution was dropped on the grid. After 20 min, the grid was washed with 10 μL of DI water 3 times. Five μL of 2% uranyl acetate water solution was put on the grid for 10 s, and a piece of filter paper was used to absorb the stain solution from the grid edge. The grid was dried in air and imaged via a JEOL JEM2100 TEM at 200 kV.

To characterize the morphology of scaffolds with confocal microscopy, RBC membrane vesicles were labeled with 1, 2-dimyristoyl-sn-glycero-3-phosphoethanolamine-N-(lissamine rhodamine B sulfonyl) (ammonium salt) (RhB-DMPE) (Avanti, Alabama), and PLGA NPs were labeled with DiD. Twenty μg of albumin–fluorescein isothiocyanate conjugate (FITC-BSA) (Sigma) was added during the scaffold preparation to label the scaffold structure. Scaffolds were rehydrated with DI water and imaged using a laser scanning confocal microscope (Olympus FluoView FV1000).

2.6 *In vivo* cell infiltration study

Female C57BL/6J mice at 8-10 weeks of age were used for the *in vivo* study. The mice were randomly divided into three groups. Each group of mice were subcutaneously injected with either blank MA-alginate scaffolds, MA-alginate scaffolds with PLGA NPs (PLGA-alginate scaffolds), or MA-alginate scaffolds with RBCM-PLGA NPs (RBCM-PLGA-alginate scaffolds) in saline. Each mouse received two of the same type of scaffolds with one in the left and one in the right flank. After 1 or 10 days, mice from each group were sacrificed, and the scaffolds were harvested. Scaffolds were digested in 1 mL collagenase II (Worthington, NJ) solution at 250 U/mL for 30 min at 37 °C. The scaffolds were then mechanically disrupted and filtered through a 70 μm nylon cell strainer (VWR). The collected cells were spun down at 1,500 × RPM for 5 min, washed with PBS, and counted using a hemocytometer. For each mouse, 0.25 million cells isolated from two scaffolds were stained for flow cytometry analysis. For staining, cells were first incubated with anti-CD16/32 (BioLegend) for 15 min at 4 °C to block Fc receptors. The cells were then stained with various antibodies including APC-conjugated CD11c (BioLegend), FITC-conjugated F4/80 (BioLegend), and PE-conjugated Ly6G (BioLegend) for 30 min at 4 °C. The stained cells were washed with 4% FBS in PBS twice before being characterized by a flow cytometer (BD Bioscience). Data were analyzed with Flowjo (Tree Star).

2.7 Real-time PCR analysis of cytokine expression

Fresh cells isolated from scaffolds were stored in TRIzol (Life Technologies), and RNA from cells was isolated using TRIzol reagent and TURBO DNA-free Kit (Invitrogen) according to manufacturer instructions. The concentration of RNA was quantified using the NanoDrop 1000 Spectro-photomer (Thermo Scientific). cDNA was prepared according to the protocol provided by the High-Capacity cDNA Reverse Transcription Kit (Applied Biosystems). qPCR was carried out using PowerUp SYBR Green Master Mix (Applied Biosystems) on QuantStudio 6 Flex Real-Time PCR System (Applied Biosystems). Primer sequences were as follows: GAPDH (F: CCAGAACATCATCCCTGCAT; R: GTTCAGCTCTGGGATGACCTT), IL10 (F: GCTCTTACTGACTGGCATGAG; R: CGCAGCTCTAGGAGCATGTG), TGF-β (F: CAACCCAGGTCCTTCCTAAA; R: GGAGAGCCCTGGATACCAAC), TNF-α (F: AGGGTCTGGGCCATAGAACT; R: CCACCACGCTCTTCTGTCTAC), and IL 12 (F: GCTTCTCCCACAGGAGGTTT; R: CTAGACAAGGGCATGCTGGT). GAPDH served as an internal control, and all data were normalized to the values of blank MA-alginate scaffolds.

2.8 Statistical analysis

Data are presented as mean ± SD or SEM. All the values in the main text indicate mean ± SD unless otherwise specified. Statistical significance between groups was analyzed using Student t-test (two-sample assuming equal variances), and $P<0.05$ was considered as significant.

3 Results and discussion

3.1 Preparation and characterization of PLGA NPs and RBCM-PLGA NPs

We fabricated PLGA NPs following a previously reported double emulsion method [29]. The DLS results showed an average PLGA NP size of 225 nm (Fig, 2(a)). RBCM vesicles with an average size of 290 nm were prepared by generating RBC ghosts from the blood of C57BL/6J mice and sonicating them. Incubation of PLGA NPs with RBCM vesicles overnight at 4 °C enabled RBCM vesicles to coat PLGA NPs, forming RBCM-PLGA NPs (Fig. 2(b)) [32]. The better known physical extrusion method expedites the process of membrane coating around NPs at the cost of reduced yield because a significant amount of NPs are often trapped on filters during extrusion. More recently, cell membrane coating has been achieved by sonicating core NPs and cell membranes at the same time [40]. Our method minimizes the components for sonication. After the coating step, RBCM-PLGA NPs were centrifuged to remove the excess RBC membranes. RBC membrane vesicles without a PLGA NP core are more difficult to spin down than RBCM-PLGA NPs [34]. By fluorescently labeling both cell membranes and PLGA NPs, we found that more than half of the excess RBC membranes were removed after being centrifuged once, while less than 2% of PLGA NPs were lost. After preparation, the average size of particles became 247 nm. The coating of RBCM vesicles on PLGA NPs was also reflected in the change in particle surface potential (Fig. 2(a)). While PLGA NPs had a surface potential of −55 eV due to the terminal carboxylic add groups, the surface potential of RBCM-PLGA NPs (−43 eV) was closer to that of RBCM vesicles (−38 eV). TEM imaging of RBCM-PLGA NPs showed core shell

strudures (Fig. 2(b)). The size of particles in the TEM image matched well with the result from DLS.

3.2 Preparation and characterization of MA-alginate scaffolds

Porous scaffolds have broad applications in tissue regeneration and immune cell modulation because connedive pores around or larger than 100 μm allow cell migration into scaffolds. To make macroporous scaffolds that can maintain their pore size, MA-alginate was employed for generating chemically crosslinked alginate. MA-alginate hydrogels have been shown to retain their shapes and macroporous structures after injection [39]. MA-alginate was prepared through the esterification reaction of methacrylic anhydride with hydroxyl groups on alginate (Fig. S1 in the Electronic Supplementary Materials (ESM)). Based on the ^{1}H NMR (Fig. S2 in the ESM), the degree of substitution was 11%. MA-alginate scaffolds were prepared by crosslinking methacrylate groups of MA-alginate via free radical reaction in the presence of APS and TEMED. The crosslinking reaction was performed at −20 °C in order to generate macroporous structures through the formation of ice crystals in the system [39]. The addition of FITC-BSA allowed for the visualization of the interconnected wall structure using confocal microscopy. The pore size of MA-alginate scaffolds were shown to be around 90 pm in the confocal images (Fig. 3). PLGA NPs and RBCM-PLGA NPs were loaded into scaffolds by rehydrating lyophilized scaffolds with NP solutions followed by a second lyophilization step to adsorb the particles to the scaffold walls. For imaging, PLGA NPs were labeled with DiD, while RBCM vesicles were labeled with RhB-DMPE. Figure 3 demonstrates that NPs were successfully loaded into the scaffolds and that the loading of NPs did not change the pore sizes. NPs were mainly located close to the scaffold frame walls. The high resolution images reveal the colocalization of PLGA NPs and RBCM vesicles, indicating the RBCM vesicles were well coated on PLGA NPs.

3.3 *In vivo* study of short-term cell infiltration in scaffolds

Scaffolds biocompatibility is one of the most important aspects determining their potential biomedical applications. Scaffolds that cause serious inflammation are non-ideal for many applications as reactive oxygen species, matrix degrading enzymes, and inflammatory cytokines damage scaffold-supported cells and tissues surrounding the scaffolds, and may even have systemic effects [21, 22]. The immune cells in contact with scaffolds play a major role in initiating inflammation, which includes both short-term and long-term responses. To study the short-term inflammatory responses from scaffolds and nanoparticles, we subcutaneously injected scaffolds into mice and characterized the cells recruited to the scaffolds one day later. The total number of cells inside PLGA-alginate and RBCM-PLGA-alginate scaffolds were 1.14 ± 0.24 million per scaffold and 0.93 ± 0.07 million per scaffold, respectively (Fig. 4(a)). There were fewer cells, 0.50 ± 0.26 million per scaffold in the blank MA-alginate scaffolds.

Alginate is inert and highly biocompatible as reported in many references [39]; however, the incorporation of nanoparticles increased the number of cells interacting with scaffolds. We identified $CD11c^{+}F4/80^{-}$ cells as dendritic cells (DCs), $F4/80^{+}$ cells as monocytes/macrophages, and $Ly6G^{+}$ cells as neutrophils. The gating strategy for each cell type is shown in Figure S3 in the ESM. Figure 4(b) shows a representative scatter plot of cells

isolated from PLGA-alginate scaffolds. After the introduction of scaffolds into animals or humans, neutrophils are first recruited and are associated with acute inflammation [21, 22]. The addition of PLGA NPs into MA-alginate scaffolds increased the percentage of neutrophils threefold from 14.96 ± 5.58% to 52.12 ± 8.98% (Fig. 4(c)), and the absolute number of neutrophils increased fivefold from 0.11 ± 0.08 million per scaffold to 0.58 ± 0.11 million per scaffold. Notably, RBC membrane coating of PLGA NPs eliminated the inflammatory effect of PLGA NPs on neutrophil recruitment as the percentage and absolute number of neutrophils fell back to the similar levels as in blank MA-alginate scaffolds. The existence of PLGA NPs and RBCM-PLGA NPs inside MA alginate scaffolds did not have major effects on the DC population. Although the incorporation of either NPs reduced the percentages of DCs by half, the number of DCs remained similar among the three different scaffolds. The addition of PLGA NPs into MA-alginate scaffolds significantly reduced the percentage of monocytes/macrophages from 44.63 ± 1.65% to 12.7 ± 4.44%. It also attenuated the cell number from 0.22 ± 0.12 million per scaffold to 0.14 ± 0.04 million per scaffold. The RBC membrane coating of PLGA NPs resulted in an increased percentage of monocytes/macrophages (28.15 ± 1.39%) and cell number (0.26 ± 0.04 million per scaffold), bringing the numbers closer to the condition without any NPs. The significantly higher number of neutrophils in the scaffolds with PLGA NPs indicates that PLGA NPs are not as biocompatible as alginate possibly due to their hydrophobidty that leads to relatively higher protein adsorption and complement pathway activation. However, coating PLGA NPs with RBC membranes from the same strain of mice were able to camouflage the particles from the immune system and significantly reduced the number of infiltrating neutrophils.

3.4. Analysis of cytokine expression by cells in scaffolds

Another indicator of inflammation is cellular expression of inflammatory cytokines. Therefore, we quantified various cytokine mRNA transcripts from scaffold cells one day after scaffold injection, including pro-inflammatory cytokines IL-12 and TNF-α, and anti-inflammatory cytokines IL-10 and TFG-β. For pro-inflammatory cytokines, the expression of IL-12 and TNF-α in cells from PLGA-alginate scaffolds increased threefold over cells from blank MA-alginate scaffolds, while the cells from RBCM-PLGA-alginate scaffolds showed similar mRNA expression of pro-inflammatory cytokines as those from blank MA-alginate scaffold cells (Fig. 5(a)). For anti-inflammatory cytokines, the cells in PLGA-alginate scaffolds expressed around 50% less IL-10 compared with cells in blank MA-alginate scaffolds. IL-10 expression in the cells from RBCM-PLGA-alginate scaffolds was approximately 80% of that in blank MA-alginate scaffolds (Fig. 5(b)). The expression of TGF-β was similar among all three types of scaffolds (Fig. 5(b)). Overall, the incorporation of PLGA NPs into MA-alginate scaffolds significantly increased the expressions of pro-inflammatory cytokine, IL-12 and TNF-α and decreased the expressions of anti-inflammatory cytokine, IL-10. However, RBC membrane coating could rescue the cytokine environment by reducing the expression of IL-12 and TNF-α mRNA to levels similar to those in blank MA-alginate scaffolds and increasing the expression of anti-inflammatory cytokine IL-10 mRNA.

3.5. Longer-term *in vivo* cell infiltration study in scaffolds

Next we studied the phenotypes of cells recruited to scaffolds 10 days after scaffold injection. Compared with the 1 day experiment, total cell numbers in all three types of scaffolds decreased, with PLGA-alginate scaffolds having the most cells (0.72 ± 0.13 million per scaffold) and blank MA-alginate scaffolds having the fewest cells (0.36 ± 0.10 million per scaffold) (Fig. 6(a)). The percentages of neutrophils were less than 1%, and their absolute numbers were less than 10,000 for each of the three types of scaffolds (Fig. 6(b), 6(c), and 6(d)). The significant decrease of neutrophil numbers compared with those at day 1 is consistent with the fact that neutrophils are the first cells migrating to inflammatory areas, and the cell number peaks quickly within 1 or 2 days [21, 22]. Compared with those in the 1 day experiment, the percentages of macrophages in all three types of scaffolds increased by 20-30%, with blank MA-alginate scaffolds having the highest percentage at 64.95 ± 6.53%. As for the macrophage numbers, RBCM-PLGA-alginate scaffolds had the highest number of macrophages (0.33 ± 0.03 million per scaffold), while blank MA-alginate scaffolds had the lowest number (0.23 ± 0.05 million per scaffold), which were very close to those in the 1-day experiment. The percentage of DCs decreased in blank MA-alginate scaffolds and remained similar in both PLGA-alginate and RBCM-PLGA-alginate scaffolds. PLGA-alginate scaffolds showed the highest number of DCs (0.08 ± 0.03 million per scaffold) and was similar to that of the 1 day experiment. Overall, after 10 days, the number of neutrophils decreased significantly in all three types of scaffolds, directly resulting in the lower number of total cells compared with the results obtained 1 day after scaffold injection. In addition, the number of macrophages were similar in all three scaffolds. The effects to PLGA NPs and RBC membrane coating on cell recruitment diminished at day 10 likely because the small NPs had degraded or were cleared by recruited cells.

4 Conclusion

In summary, using PLGA NPs formed by double emulsion as a model particle, we have shown that nanoparticles capable of controlling therapeutic release may induce significant acute inflammatory responses to highly biocompatible scaffolds *in vivo* when nanoparticles are incorporated in scaffolds. Coating of RBC membranes around nanoparticles can eliminate the nanoparticle-induced short-term inflammatory responses to scaffold constructs, including dramatically increased neutrophil infiltration and pro-inflammatory cytokines. The incorporation of PLGA NPs and RBCM-PLGA NPs did not show an appreciable effect on the numbers of infiltrated neutrophils or macrophages in alginate scaffolds 10 days after the subcutaneous injection of the scaffolds into mice. This is possibly due to the degradation of nanoparticles or their clearance by infiltrated cells. The protection from cell membrane coating is expected to last longer for microparticles as it is more difficult for large particles to be cleared by cells and they take a longer time to degrade. Even transient protection can be pivotal because acute inflammatory responses in early stages can alter the recruited cell population and reduce the viability and function of scaffold-seeded or recruited regenerative cells. Therefore, we believe this facile approach to harnessing the natural biocompatibility of cell membranes for reducing inflammatory and foreign body responses may have applications in fields such as tissue regeneration and immune modulation.

Supplementary Material

Refer to Web version on PubMed Central for supplementary material.

Acknowledgements

Research reported in this publication was supported by a faculty startup fund from Drexel University to H.C., a pilot grant from the Clinical & Translational Research Institute (CTRI), and National Institute of Allergy and Infectious Diseases of the National Institutes of Health under Award Number R21AI133372. We would like to thank Dr. Elizabeth Blankenhorn and Dr. Frank Bearoff for their help on real-time PCR analysis.

References

[1]. Teng YD; Lavik EB; Qu XL; Park KI; Ourednik J; Zurakowski D; Langer R; Snyder EY Functional recovery following traumatic spinal cord injury mediated by a unique polymer scaffold seeded with neural stem cells. Proc. Natl. Acad. Sci. U. S. A 2002, 99, 3024–3029. [PubMed: 11867737]

[2]. Li WJ; Tuli R; Okafor C; Derfoul A; Danielson KG Hall DJ; Tuan RS A three-dimensional nanofibrous scaffold for cartilage tissue engineering using human mesenchymal stem cells. Biomaterials 2005, 26, 599–609. [PubMed: 15282138]

[3]. Ali OA; Huebsch N; Cao L; Dranoff G; Mooney DJ Infection-mimicking materials to program dendritic cells in situ. Nat. Mater. 2009, 8, 151–158. [PubMed: 19136947]

[4]. Sheridan MH; Shea LD; Peters MC; Mooney DJ Bioadsorbable polymer scaffolds for tissue engineering capable of sustained growth factor delivery. J. Control. Release 2000, 64, 91–102. [PubMed: 10640648]

[5]. Lee KY; Peters MC; Anderson KW; Mooney DJ Controlled growth factor release from synthetic extracellular matrices. Nature 2000, 408, 998–1000. [PubMed: 11140690]

[6]. Lutolf MR; Weber FE; Schmoekel HG; Schense J; Kohler T; Muller R; Hubbell JA Repair of bone defects using synthetic mimetics of collagenous extracellular matrices. Nat. Biotechnol. 2003, 21, 513–518. [PubMed: 12704396]

[7]. Elbert DL; Pratt AB; Lutolf MP; Halstenberg S; Hubbell JA Protein delivery from materials formed by self-selective conjugate addition reactions. J. Control. Release 2001, 76, 11–25. [PubMed: 11532309]

[8]. Seliktar D; Zisch AH; Lutolf MP; Wrana JL; Hubbell JA MMP-2 sensitive, VEGF-bearing bioactive hydrogels for promotion of vascular healing. J. Biomed. Mater. Res. Part A 2004, 68A, 704–716.

[9]. Martino MM; Briquez PS; Ranga A; Lutolf MP; Hubbell JA Heparin-binding domain of fibrin(ogen) binds growth factors and promotes tissue repair when incorporated within a synthetic matrix. Proc. Natl. Acad. Sci. U. S. A 2013, 110, 4563–4568. [PubMed: 23487783]

[10]. Purcell BP; Lobb D; Charati MB; Dorsey SM; Wade RJ; Zellars KN; Doviak H; Pettaway S; Logdon CB; Shuman JA; Freels PD; Gorman JH; Gorman RC; Spinale F; Burdick JA Injectable and bioresponsive hydrogels for on-demand matrix metalloproteinase inhibition. Nat. Mater. 2014, 13, 653–661. [PubMed: 24681647]

[11]. Richardson TP; Peters MC; Ennett AB; Mooney DJ Polymeric system for dual growth factor delivery. Nat. Biotechnol. 2001, 19, 1029–1034. [PubMed: 11689847]

[12]. Li SR; Nih LR; Bachman H; Fei P; Li YL; Nam E; Dimatteo; Carmichael ST; Barker TH; Segura T Hydrogels with precisely controlled integrin activation dictate vascular patterning and permeability. Nat. Mater 2017, 16, 953–961. [PubMed: 28783156]

[13]. Vacanti NM; Cheng H; Hill PS; Guerreiro JDT; Dang TT; Ma ML; Watson S; Hwang NS; Langer R ; Anderson DG Localized delivery of dexamethasone from electrospun fibers reduces the foreign body response. Biomacromolecules 2012, 13, 3031–3038. [PubMed: 22920794]

[14]. Tan Q; Tang H; Hu JG; Hu YR; Zhou XM; Tao YM; Wu ZS Controlled release of chito san/ heparin nanoparticle-delivered VEGF enhances regeneration of decellularized tissue-engineered scaffolds. Int. J. Nanomed 2011, 6, 929–942.

[15]. Holland TA; Bodde EWH; Cuijpers V; Baggett LS; Tabata Y; Mikos AG; Jansen JA Degradable hydrogel scaffolds for in vivo delivery of single and dual growth factors in cartilage repair. Osteoarthritis Cartilage 2007, 15, 187–197. [PubMed: 16965923]

[16]. Hosseinkhani H; Hosseinkhani M; Gabrielson NP; Pack DW; Kliademliosseini A; Kobayashi H DNA nanoparticles encapsulated in 3D tissue-engineered scaffolds enhance osteogenic differentiation of mesenchymal stem cells. J. Biomed. Mater Res. Part A 2008, 85A, 47–60.

[17]. Hedberg EL; Tang A; Crowther RS; Carney DH ; Mikos AG Controlled release of an osteogenic peptide from injectable biodegradable polymeric composites. J. Control. Release 2002, 84, 137–150. [PubMed: 12468217]

[18]. Verbeke CS; Gordo S; Schubert DA; Lewin SA; Desai RM; Dobbins J; Wucherpfemiig KW; Mooney DJ Multicomponent injectable hydrogels for antigen-specific tolerogenic immune modulation. Adv. Healthc. Mater 2017, 6, 15.

[19]. Gurtner GC; Werner S; Barrandon Y; Longaker MT Wound repair and regeneration. Nature 2008, 453, 314–321. [PubMed: 18480812]

[20]. Anderson JM; Rodriguez A; Chang DT Foreign body reaction to biomaterials. Semin. Immunol. 2008, 20, 86–100. [PubMed: 18162407]

[21]. Anderson JM Biological responses to materials. Ann. Rev. Mater Res. 2001, 31, 81–110.

[22]. Anderson J; McNally A Biocompatibility of implants: lymphocyte/macrophage interactions. Semin. Immunopathol. 2011, 33, 221–233. [PubMed: 21271251]

[23]. Kim YK; Chen EY; Liu WF Biomolecular strategies to modulate the macrophage response to implanted materials. J. Mat. Chem. B 2016, 4, 1600–1609.

[24]. Zhang L; Cao ZQ; Bai T; Carr L; Ella-Menye JR; Irvin C; Ratner BD; Jiang SY Zwitterionic hydrogels implanted in mice resist the foreign-body reaction. Nat. Bioteclmol. 2013, 31, 553–556.

[25]. Vegas AJ; Veiseh O; Doloff JC; Ma ML; Tam HH; Bratlie K; Li J; Bader AR; Langan E; Olejnik K; Fenton P; Kang JW; Hollister-Locke J; Bochenek MA; Chiu A; Siebert S; Tang K; Jhunjhunwala S; Aresta-Dasilva S; Dholakia N; Thakrar R; Vietti T; Chen M; Cohen J; Siniakowicz K; Qi MRG; McGarrigle J; Lyle S; Harlan DM; Greiner DL; Oberholzer J; Weir GC; Langer R; Anderson DG Combinatorial hydrogel library enables identification of materials that mitigate the foreign body response in primates. Nat. Bioteclmol. 2016, 34, 345–352.

[26]. Chen EY; Chu SH; Gov L; Kim YK; Lodoen MB; Tenner AJ; Liu WF CD200 modulates macrophage cytokine secretion and phagocytosis in response to poly(lactic-co-glycolic acid)microparticles and films. J. Mat. Chem. B 2017, 5, 1574–1584.

[27]. Wu YQ; Qu H; Sfyroera G; Tzekou A; Kay BK; Nilsson; Ekdahl KN; Ricklin D; Lambris JD Protection of nonself surfaces from complement attack by factor H-binding peptides: implications for therapeutic medicine (vol 186, pg 4269, 2011). J. Immunol 2012, 188, 6425–6425.

[28]. Hu CMJ; Zhang L; Aryal S; Cheung C; Fang RH; Zhang LF. Erythrocyte membrane-camouflaged polymeric nanoparticles as a biomimetic delivery platform. Proc. Natl. Acad. Sci. U. S. A 2011, 108, 10980–10985. [PubMed: 21690347]

[29]. Hu CMJ; Fang RH; Wang KC; Luk BT; Thamphiwatana S; Dehaini D; Nguyen P; Angsantikul P; Wen CH; Kroll AV; Carpenter C; Ramesh M; Qu V; Patel SH; Zhu J; Shi W; Hofman FM; Chen TC; Gao WW; Zhang K; Chien S; Zhang LF Nanoparticle biointerfacing by platelet membrane cloaking. Nature 2015, 526, 118–121. [PubMed: 26374997]

[30]. Hu QY; Sun WJ; Qian CG; Wang C; Bomba HN; Gu Z Anticancer platelet-mimicking nanovehicles. Adv. Mater. 2015, 27, 7043–7050. [PubMed: 26416431]

[31]. Gao M; Liang C; Song XJ; Chen Q; Jin QT; Wang C; Liu Z. Erythrocyte-membrane-enveloped perfluorocarbon as nanoscale artificial red blood cells to relieve tumor hypoxia and enhance cancer radiotherapy. Adv. Mater. 2017, 29, 1701429

[32]. Fan ZY; Zhou H; Li PY; Speer JE; Cheng H Structural elucidation of cell membrane-derived nanoparticles using molecular probes. J. Mat. Chem. B 2014, 2, 8231–8238.

[33]. Zhou H; Fan ZY; Lemons PK; .Cheng H A facile approach to functionalize cell membrane-coated nanoparticles. Theranostics 2016, 6, 1012–1022. [PubMed: 27217834]

[34]. Fang RH; Hu CMJ; Luk BT; Gao WW; Copp JA; Tai YY; O'Connor DE.; Zhang LF. Cancer cell membrane-coated nanoparticles for anticancer vaccination and drug delivery. Nano Lett. 2014, 14, 2181–2188. [PubMed: 24673373]

[35]. Xuan M; Shao J; Zhao J; Li Q; Dai L; Li J Red blood cell membranes cloaked magnetic mesoporous silica nanoparticles applied for cancer therapy. Angewandte Chemie (International ed. in English) 2018, 10.1002/anie.201712996.

[36]. Li PY; Fan ZY; Cheng H Cell membrane bioconjugation and membrane-derived nanomaterials for immunotherapy. Bioconjugate chemistry 2018, 29, 624–634. [PubMed: 29323870]

[37]. Fang RH; Kroll AV; Gao W; Zhang L Cell membrane coating nanotechnology. Adv. Mater. 2018, 10.1002/adma.201706759, e1706759. [PubMed: 29582476]

[38]. Oldenborg PA; Zheleznyak A; Fang YF; Lagenaur CF; Gresham HD; Lindberg FP Role of CD47 as a marker of self on red blood cells. Science 2000, 288, 2051–2054. [PubMed: 10856220]

[39]. Bencherif SA; Sands RW; Bhatta D; Arany P; Verbeke CS; Edwards DA; Mooney DJ Injectable preformed scaffolds with shape-memory properties. Proc. Natl. Acad. Sci. U. S. A 2012, 109, 19590–19595. [PubMed: 23150549]

[40]. Copp JA; Fang RH; Luk BT; Hu CMJ; Gao WW; Zhang K; Zhang LF Clearance of pathological antibodies using biomimetic nanoparticles. Proc. Natl. Acad. Sci. U. S. A 2014, 111, 13481–13486. [PubMed: 25197051]

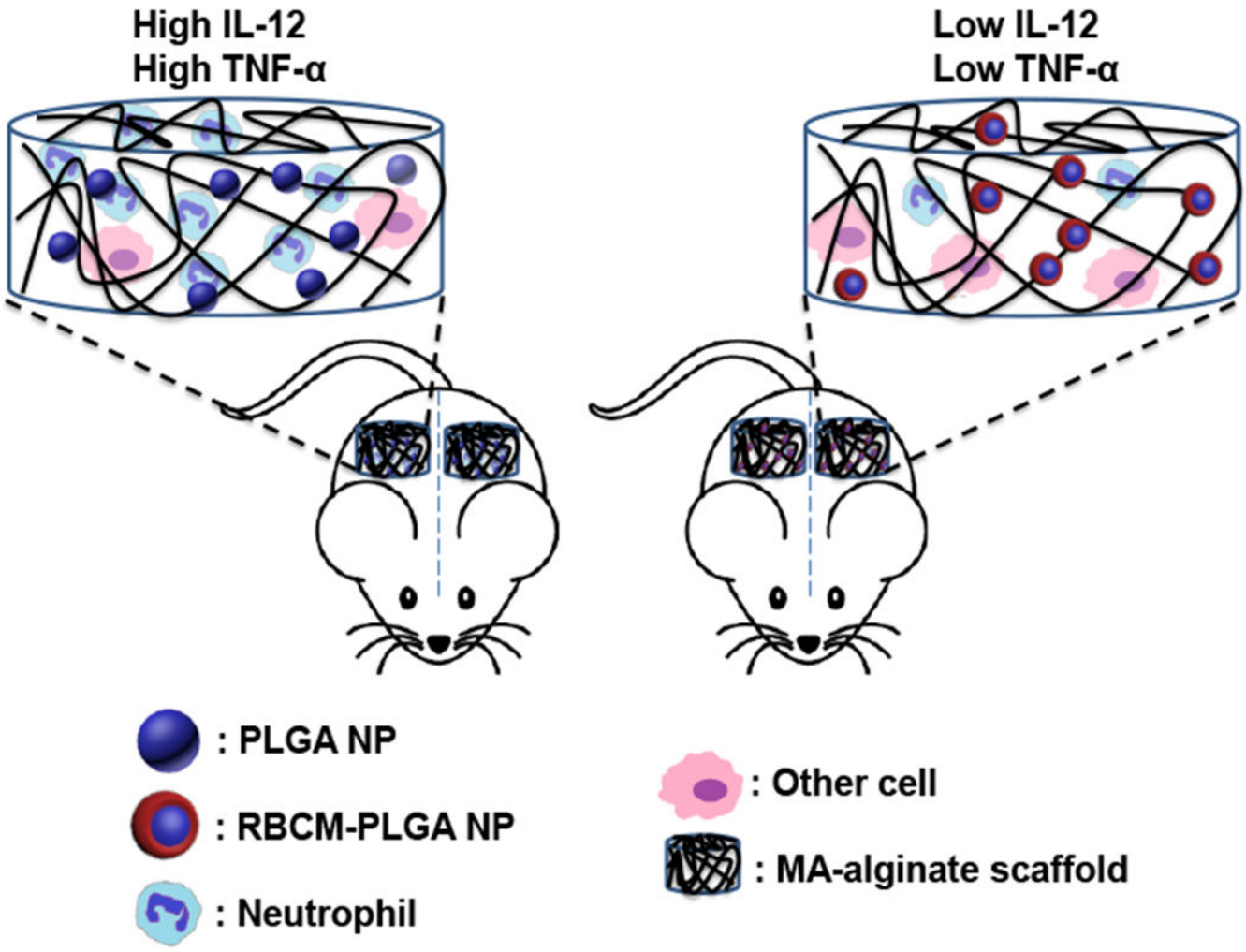

Figure 1.
A schematic illustration of reduced inflammatory response to scaffold constructs after red blood cell membrane coating on nanoparticle.

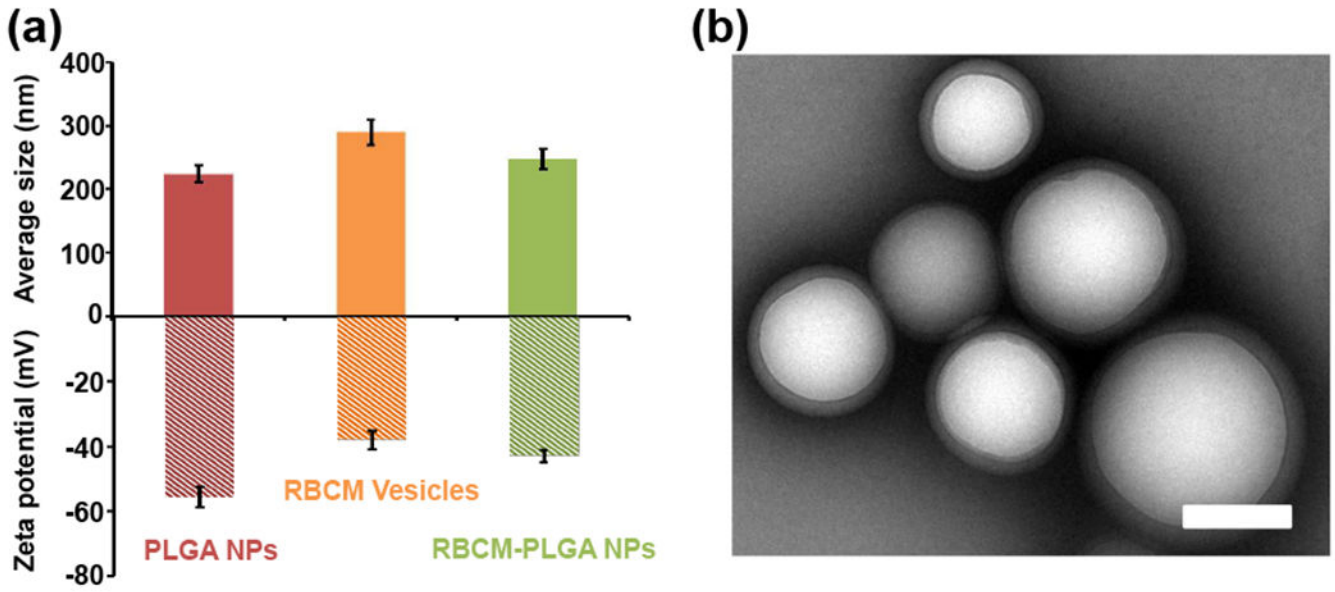

Figure 2.

Characterization of PLGA NPs and RBCM-PLGA NPs. (a) Average sizes and zeta potentials of PLGA NPs, RBC membrane vesicles, and RBCM-PLGA NPs. Values indicate mean ± SD (n=3). (b) A representative TEM image of RBCM-PLGA NPs showing a core-shell structure. Scale bar: 200 nm.

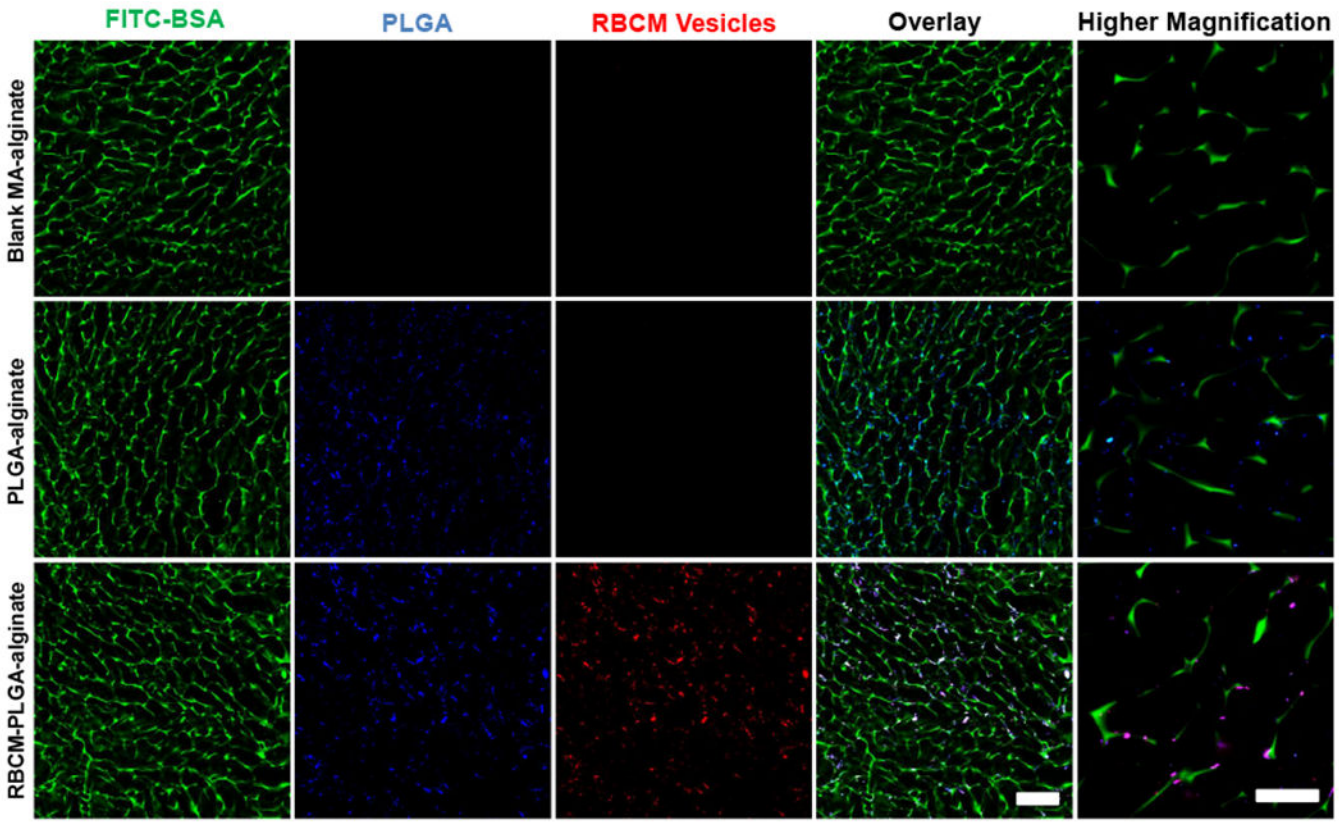

Figure 3.

Representative confocal microscopy images of blank MA-alginate, PLGA-alginate, and RBCM-PLGA-alginate scaffolds. FITC-BSA was added to the MA-alginate solution prior to cryogelation in order to label the scaffold macroporous structure. PLGA NP cores were labeled with DiD, and RBC membranes were labeled with RhB-DMPE. Scale bar for overlay: 200 μm and scale bar for higher magnification: 50 μm.

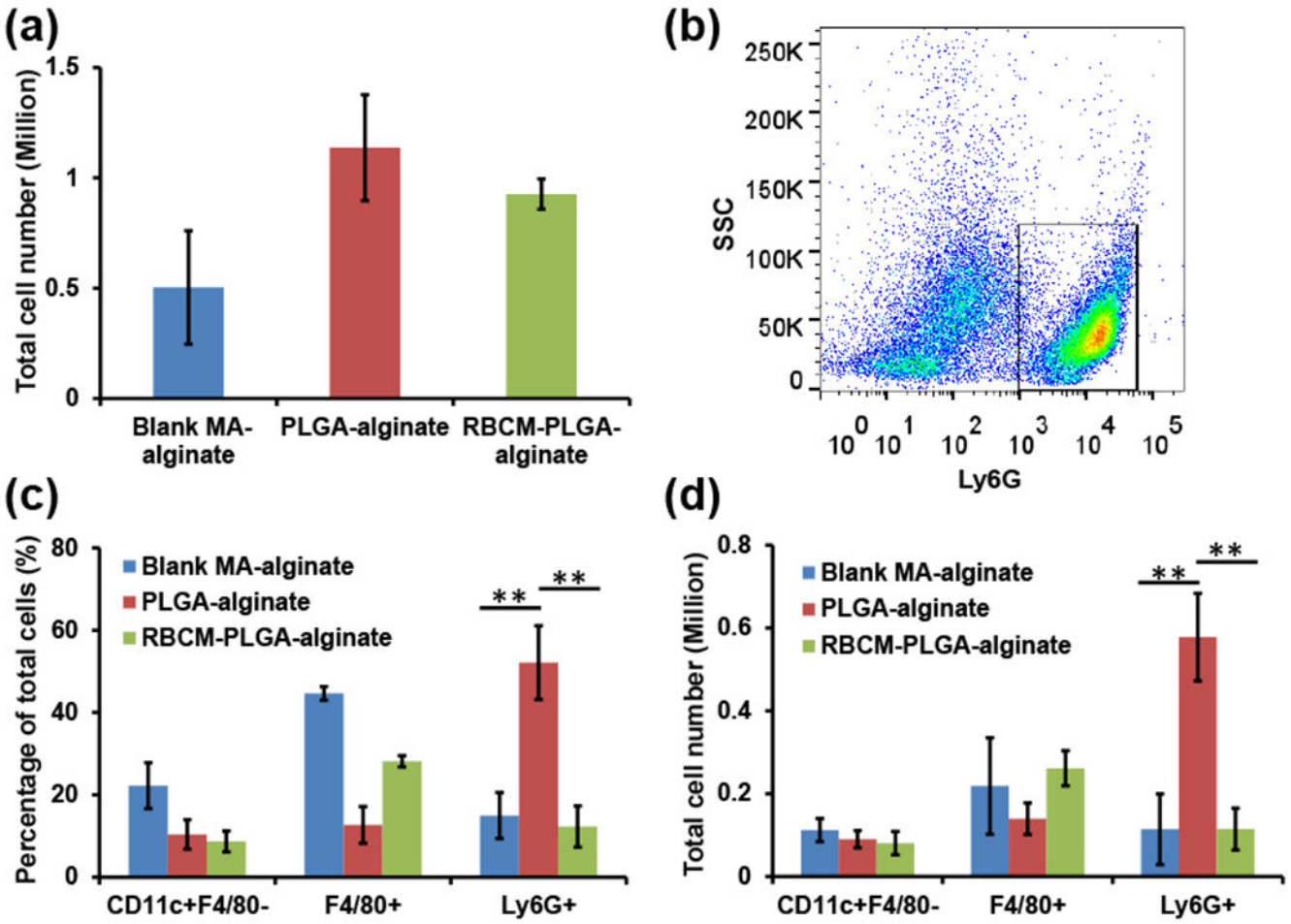

Figure 4.

Quantification of infiltrating cells inside blank MA-alginate, PLGA-alginate, and RBCM-PLGA-alginate scaffolds on day 1 after scaffold administration. Scaffolds were subcutaneously injected into mice. After 1 day, scaffold cells were harvested, and their surface markers were stained and analyzed by flow cytometry. (a) Total cell numbers in each type of scaffold. (b) A representative gating of cells from PLGA-alginate scaffolds with Ly6G as X axis and side scatter as Y axis. The black rectangle designates $Ly6G^+$ cells. (c) The percentage of $CD11c^+F4/80^-$cells, $F4/80^+$ cells, and $Ly6G^+$ cells among total cells in the three types of scaffolds. (d) The number of $CD11c^+F4/80^-$ cells, $F4/80^+$ cells, and $Ly6G^+$ cells present in the three types of scaffolds. Values indicate mean ± SD (n=3). **, $P < 0.01$.

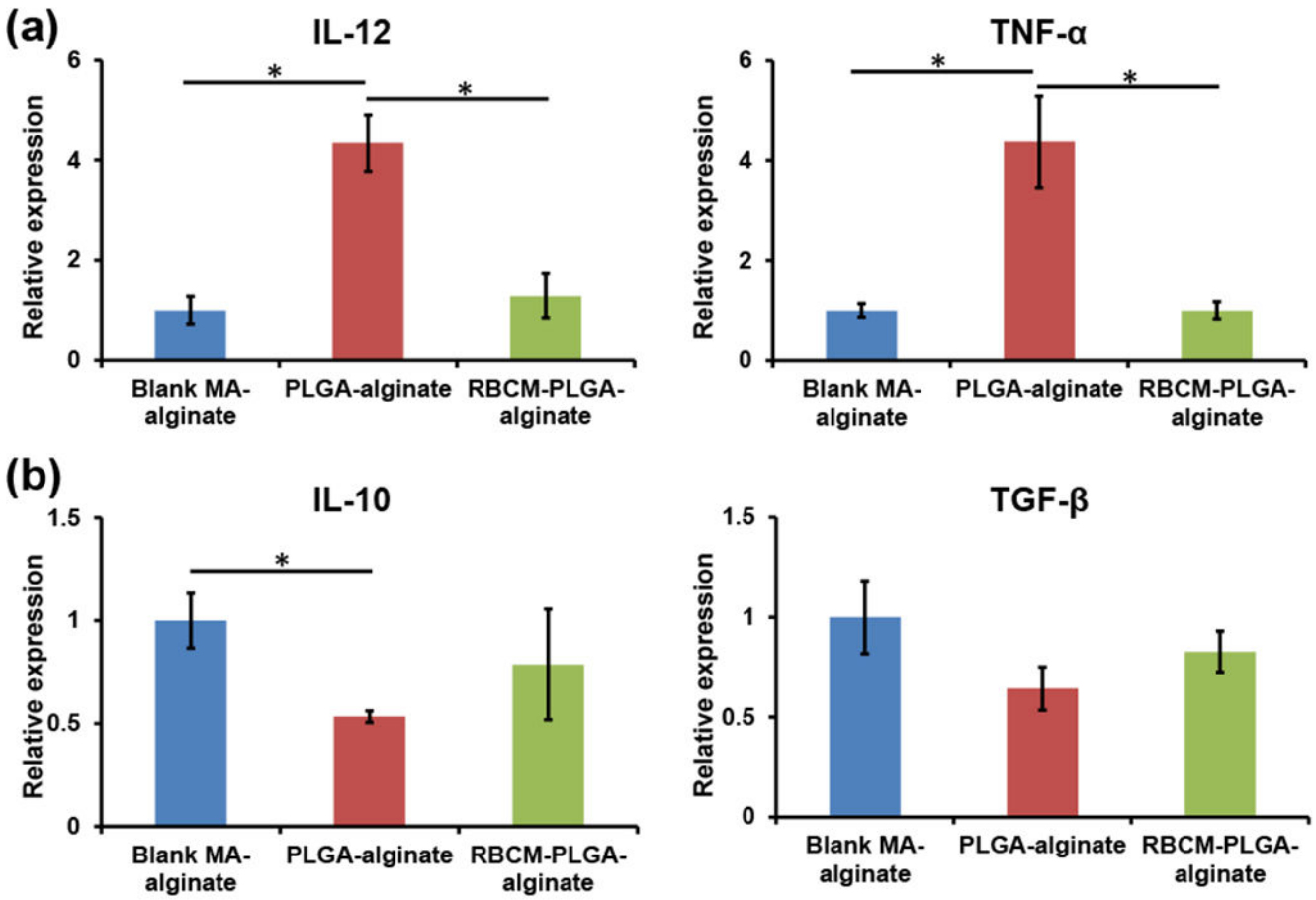

Figure 5.

RT-PCR analysis of cytokine mRNA expression in the cells isolated from blank MA-alginate, PLGA-alginate, or RBCM-PLGA-alginate scaffolds on day 1 after scaffold injection. (a) mRNA expressions of pro-inflammatory cytokine IL-12 and TNFα. (b) mRNA expression of anti-inflammatory cytokine IL-10 and TGF-β. Values indicate mean ± SEM (n=3). *, $P < 0.05$.

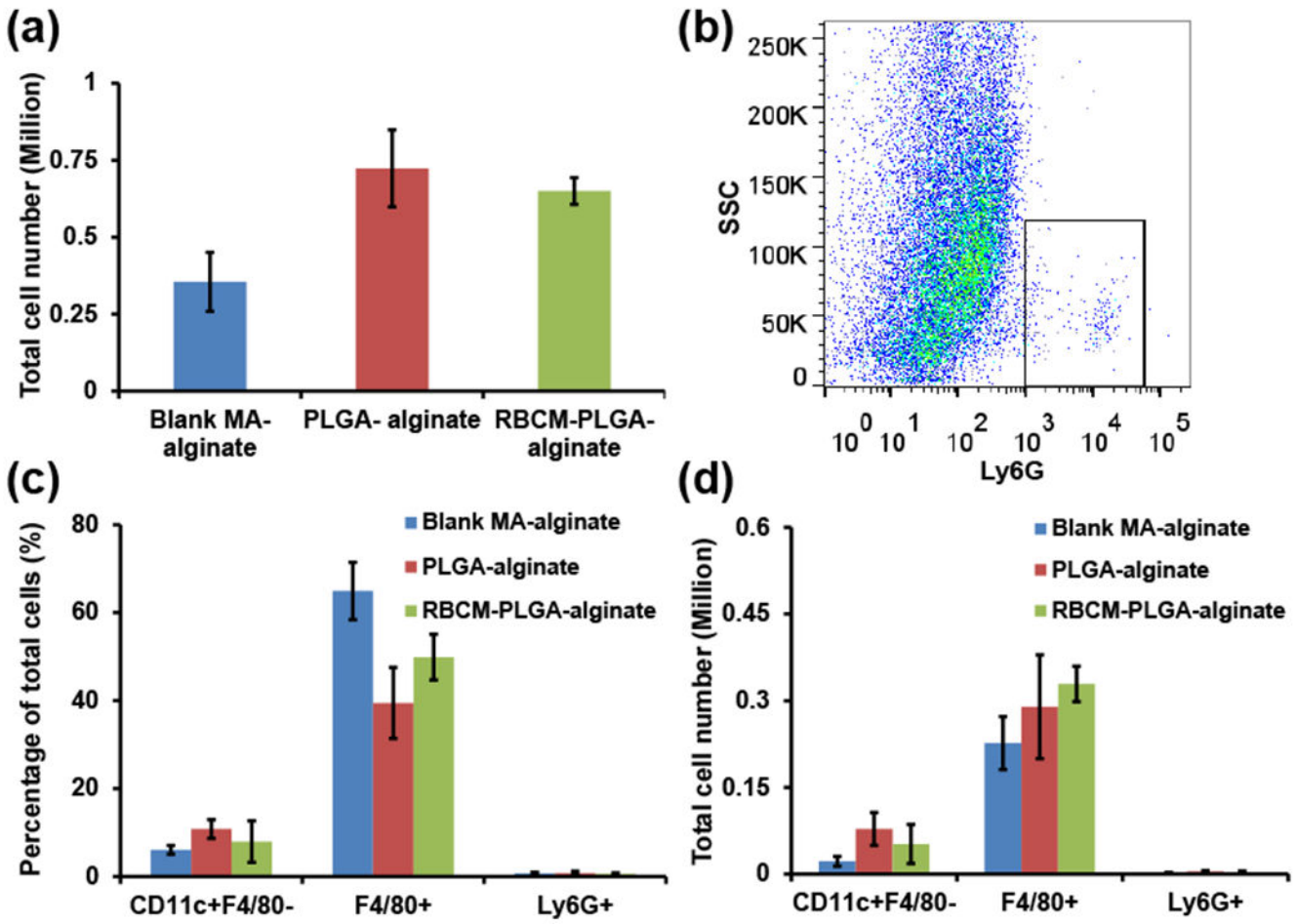

Figure 6.

Quantification of infiltrating cells inside blank MA-alginate, PLGA-alginate, and RBCM-PLGA-alginate scaffolds on day 10 after scaffold administration. Scaffolds were subcutaneously injected into mice. The isolated cells were stained for surface markers and analyzed by flow cytometry. (a) Total cell numbers in each type of scaffold. (b) A representative gating of cells from PLGA-alginate scaffolds with Ly6G as X axis and side scatter as Y axis. The black rectangle designates $Ly6G^+$ cells. (c) The percentage of $CD11c^+F4/80^-$ cells, $F4/80^+$ cells, and $Ly6G^+$ cells among total cells. (d) The number of $CD11c^+F4/80^-$ cells, $F4/80^+$ cells, and $Ly6G^+$ cells. Values indicate mean ± SD (n=3).